Eur. Phys. J. B **20**, 141–149 (2001)

THE EUROPEAN PHYSICAL JOURNAL B

EDP Sciences

Lattice Boltzmann model for magnetic fluid interfaces

V. Sofonea[1,2,3] and W.-G. Früh[2,a]

[1] Laboratory for Numerical Simulation and Parallel Computing in Fluid Mechanics, Centre for Fundamental and Advanced Technical Research, Romanian Academy, Bd. Mihai Viteazul 24, 1900 Timişoara, Romania
[2] Department of Mechanical and Chemical Engineering, James Nasmyth Building, Heriot-Watt University, Riccarton, Edinburgh EH14 4AS, Scotland, UK
[3] Edinburgh Parallel Computing Centre, James Clerk Maxwell Building, The University of Edinburgh, Mayfield Road, Edinburgh EH9 3JZ, Scotland, UK

Received 21 August 2000 and Received in final form 19 January 2001

Abstract. A Lattice Boltzmann model is developed to account for the competition between surface tension and dipolar interaction in magnetic fluids. The description of the interactions was kept as simple as possible to identify and isolate the nature of the essential interactions in the examined situations. The model is used thereafter in order to simulate the deformation of a magnetic fluid drop under the action of an external magnetic field, as well as the onset of the normal field instability in magnetic fluids. The success of the model, and easily identified deviations, demonstrate that the model is a powerful and versatile tool for the study of magnetic and nonmagnetic fluid systems with interfaces.

PACS. 75.50.Mm Magnetic liquids – 47.11.+j Computational methods in fluid dynamics – 47.20.Ma Interfacial instability

1 Introduction

Lattice Boltzmann (LB) cellular automata techniques have been proved to be extremely useful tools for investigating complex fluid physics (see the recent monographs [1–3] and references therein). Their parallel nature, the easy handling of irregular geometries and the possibility to incorporate the physics at a mesoscopic level are major advantages of these techniques, when compared to more classical methods for simulating fluid phenomena. Interparticle interactions, surface tension and wetting forces may be incorporated into LB models such that the macroscopic behaviour (time evolution and final equilibrium state of the system) is always recovered after performing a certain number of iterations (automaton steps).

Magnetic fluids, also known as ferrofluids (see [4–6] and references therein), are a particular class of complex fluids whose main characteristics are the presence of dipolar interactions between colloidal particles dispersed in a carrier liquid. Due to the huge number of such very small colloidal particles (approx. 100 Å in diameter) which have a permanent magnetic moment, competition between dipolar interaction and surface tension gives rise to a rich variety of interface phenomena in magnetic fluids [4,5].

This paper reports a LB model which accounts in a highly simplified form for only the principal forces which mainly define the behaviour of magnetic fluid interfaces and is organized as follows. Section 2 is a description of the 2D lattice Boltzmann model for a two component fluid system where particles belonging to one component are subjected to dipolar interaction with nearest neighbours. The influence of magnetic interaction on the linear interface profile is discussed in Section 3. The LB model is used in Section 4 to study the equilibrium shape of a magnetic fluid drop placed in a Hele-Shaw cell and subjected to an external magnetic field. An attempt to simulate the rise of the normal field (Rosensweig) instability using this model is further presented in Section 5 before final conclusions about the applicability of this model are made.

[a] e-mail: w.g.fruh@hw.ac.uk

2 Description of the Lattice Boltzmann model

Following the general approach in [7], we consider the LB evolution equation for a fluid system with two immiscible components on a square lattice $\mathcal{L}$ with unit spacing (the D2Q9 model [8]):

$$n_a^\sigma(\mathbf{x}+\mathbf{e}_a, t+1) - n_a^\sigma(\mathbf{x},t) = -\frac{1}{\tau_\sigma}\left[n_a^\sigma(\mathbf{x},t) - n_a^{\sigma,\mathrm{eq}}(\mathbf{x},t)\right]. \tag{1}$$

Here $n_a^\sigma(\mathbf{x},t)$, $\sigma = 0,1$, $\mathbf{x} \in \mathcal{L}$, is the particle number density of the component σ having the velocity

$$\mathbf{e}_a = \begin{cases} (0;0) & a = 0 \\ \left(\cos\frac{(a-1)\pi}{2}; \sin\frac{(a-1)\pi}{2}\right) & a = 1,\ldots,4 \\ \sqrt{2}\left(\cos\frac{(2a-9)\pi}{4}; \sin\frac{(2a-9)\pi}{4}\right) & a = 5,\ldots,8 \end{cases} \tag{2}$$

while $n_a^{\sigma,\mathrm{eq}}(\mathbf{x},t)$ is the corresponding equilibrium distribution function and τ_σ is the corresponding relaxation time. The equilibrium distribution functions are expressed as series expansions in the local velocity $\mathbf{u}^\sigma = \mathbf{u}^\sigma(\mathbf{x},t)$ while the series coefficients are recovered after convenient discretisation of the continuous Boltzmann equation and the recovery of hydrodynamic momenta up to fourth order in $\mathbf{u}^\sigma$ [9]:

$$n_a^{\sigma,\mathrm{eq}} = \omega_a \rho^\sigma \left[1 + 3\mathbf{e}_a \cdot \mathbf{u}^\sigma + \frac{9(\mathbf{e}_a \cdot \mathbf{u}^\sigma)^2}{2} - \frac{3}{2}(\mathbf{u}^\sigma)^2\right]. \tag{3}$$

Here

$$\omega_a = \begin{cases} \frac{4}{9}, & a = 0 \\ \frac{1}{9}, & a = 1,\ldots,4 \\ \frac{1}{36}, & a = 5,\ldots,8 \end{cases} \tag{4}$$

are the weight coefficients [9], and

$$\rho^\sigma = \sum_a n_a^\sigma \tag{5}$$

is the local number density of component σ.

The local velocity $\mathbf{u}^\sigma$ in the expression of the equilibrium distribution functions (3) is given by [7]

$$\mathbf{u}^\sigma = \mathbf{u} + \tau^\sigma \mathbf{F}^\sigma / \rho^\sigma \tag{6}$$

where

$$\mathbf{u} = \frac{\sum_\sigma (1/\tau^\sigma) \sum_a n_a^\sigma \mathbf{e}_a}{\sum_\sigma \rho^\sigma / \tau^\sigma}\,. \tag{7}$$

For simplicity, we consider that the masses of the two particle species in the system are identical and equal the unit mass. For the same reason, we used equal values of the relaxation times ($\tau_0 = \tau_1 = 1$) during all computer simulations discussed in this paper, which means that both fluid components share the same viscosity [7–12]. Note that some authors add a 1/2 factor to the term $\tau^\sigma \mathbf{F}^\sigma$ in (6); since this factor may be absorbed in the constants entering the force terms in equation (8) below, we shall not consider it here.

The total force field $\mathbf{F}^\sigma$ acting on component σ has two terms:

$$\mathbf{F}^\sigma = \mathbf{F}^{\mathrm{s},\sigma} + \mathbf{F}^{\mathrm{d},\sigma}. \tag{8}$$

The first one is responsible for the phase separation of the binary fluid system and has the form first suggested in [7]

$$\mathbf{F}^{\mathrm{s},\sigma}(\mathbf{x}) = -\rho^\sigma(\mathbf{x}) \sum_a \mathcal{G}_a^{\mathrm{s}} \rho^{\bar\sigma}(\mathbf{x} + \mathbf{e}_a)\mathbf{e}_a \tag{9}$$

where $\sigma = 0, 1$ and $\bar\sigma = 1 - \sigma$. In order to account for the correct value of the repulsive force between the two fluid components when dealing with a square lattice [10–12], we set

$$\mathcal{G}_a^{\mathrm{s}} = \omega_a \mathcal{G}, \quad a = 1,\ldots,8. \tag{10}$$

The second term in (8) accounts for the dipolar interaction which is considered to act only between particles belonging to the first component ($\sigma = 0$). These particles are supposed to be identical and carry the same permanent magnetic moment $\mathbf{m}$, whose magnitude is m. Consequently,

$$\mathbf{F}^{\mathrm{d},\sigma}(\mathbf{x}) = \begin{cases} -\rho^\sigma(\mathbf{x}) \sum_a \mathcal{G}_a^{\mathrm{d}} \rho^\sigma(\mathbf{x} + \mathbf{e}_a)\mathbf{e}_a & (\sigma = 0) \\ 0 & (\sigma = 1) \end{cases} \tag{11}$$

where

$$\mathcal{G}_a^{\mathrm{d}} = \omega_a \left[\frac{m^2}{|\mathbf{e}_a|^3} - \frac{3(\mathbf{m}\cdot\mathbf{e}_a)^2}{|\mathbf{e}_a|^5}\right] \quad a = 1,\ldots,8. \tag{12}$$

The constants $\mathcal{G}_a^{\mathrm{d}}$, which were initially defined in [13] on a hexagonal lattice, were multiplied here by the weight factors ω_a in order to account for the square lattice. Note that in the present model, unlike the model in [13], all magnetic particles carry the same magnetic moment, a simplification which reduces significantly the number of species of particles in the LB model, a fact which allows a considerable reduction in the computational effort.

3 Linear interface

3.1 Interface between two nonmagnetic fluids

The main characteristic of this model is to produce phase separation when the value of the constant $\mathcal{G}$ in (10) exceeds a critical value [7,10–12] which allows the repulsive interaction energy to win out over the thermal energy which tends to mix the particles. However, the two components are never completely separated: in each phase, one of the two components predominates while a small amount of particles belonging to the other component is still present. This is a characteristic of regular binary solutions whose components have a repulsive interaction energy proportional to their local densities [14] and is also encountered in other LB models [15–17] for binary fluid systems. The separation of the two components is better for larger values of the repulsive interaction constant $\mathcal{G}$, as seen in Figure 1 where the variation of the density ρ^0 of component $\sigma = 0$ along the x axis is shown for $\mathcal{G} = 1.5$ and $\mathcal{G} = 2.0$, when no dipolar interaction is present ($m = 0$).

The results in Figure 1 were obtained on a 256×16 lattice using periodic boundary conditions in both directions. For this reason, two symmetric plane interfaces are established in the system, but in Figure 1 we show the density profiles across a restricted interval along the x-direction (where only one of the two interfaces is visible) in order to improve the readability of the graph. Although the left phase in Figure 1 is rich in the component $\sigma = 0$, the total density $\rho = \rho^0 + \rho^1$ is found to have the same value in each phase (except the interface region [7,17]), which equilibrates the total ideal gas pressure $p_{\mathrm{i}} = \rho/3$ in bulk phases.

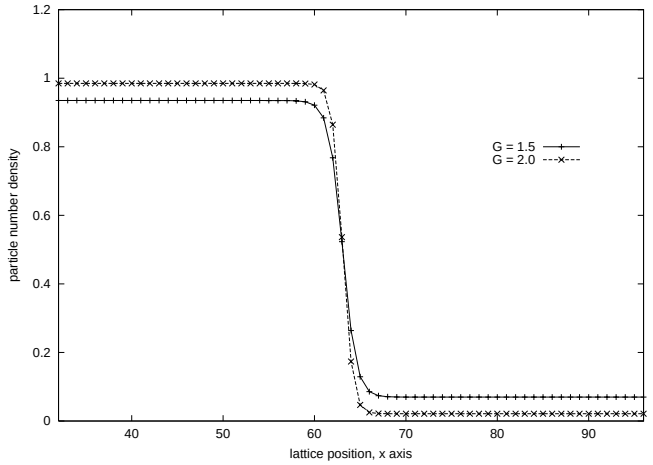

Fig. 1. Particle number density profiles of component $\sigma = 0$ across an equilibrated linear interface, for $\mathcal{G} = 1.5$ and $\mathcal{G} = 2.0$, when no dipolar interaction is present.

We should mention here that it is not possible to increase indefinitely the value of the interaction constant $\mathcal{G}$ if one wants to enhance the separation of the two fluid components in the present LB model. When exceeding a threshold value $\mathcal{G}_{\rm t}$ (which is approximately $\mathcal{G}_{\rm t} = 3.0$ in the absence of dipolar interaction), the system becomes unstable and negative values of the equilibrium distribution functions are recovered because of the large values of the local velocity which are established in this case. The presence of dipolar interactions is always found to reduce this threshold value when increasing the magnitude of the magnetic moment m. For this reason, most of our subsequent simulations were done using the values $\mathcal{G} = 1.5$ and $\mathcal{G} = 2.0$, which allow to use relatively large values for m and thus, leaves the possibility to study the effects of the competition between surface tension and dipolar forces without getting the LB particle system into the numerically unstable domain.

3.2 Interface between a magnetic and a nonmagnetic fluid

The presence of magnetic dipolar interactions alters the energy (or pressure) balance between the magnetic and nonmagnetic fluid phase, resulting in a pressure and density equilibrium which depends on the strength and orientation of the magnetisation. In this section, the equilibrium pressures of the magnetic and non-magnetic phases are derived, first from the energy levels of an array of uniform magnetic dipoles on a lattice under the influence of an externally applied field, H_0, and then based on the actual formulation of the dipolar interactions in the lattice Boltzmann model as given in equations (11) and (12). The latter predictions are then compared with results from model integrations.

Two energy terms enter the pressure balance equation, the energy of a dipole under the influence of the externally applied magnetic field and the interaction energy

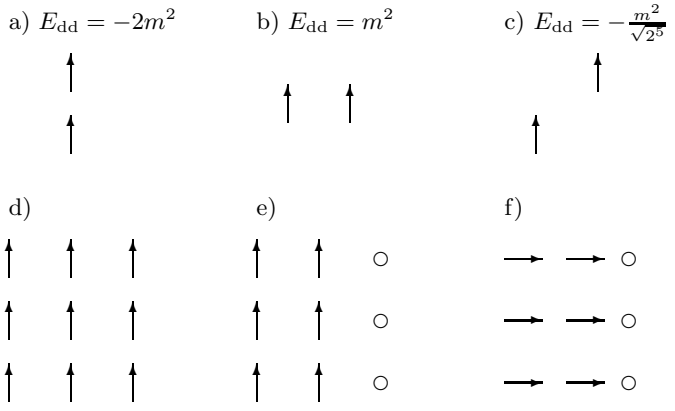

Fig. 2. Illustration of the interaction energy between a number of dipoles.

between pairs of dipoles within the fluid. The additional term describing interfacial tension present in a real system is absent in the model presented here, because the phase separation is described in a way which adds an equal term to the energy of both phases. In a pressure balance, the contribution from the separation force will then cancel out.

The energy of a point dipole with fixed magnetic moment, $\mathbf{m}$, within an applied magnetic field, $\mathbf{H}$, is given by ([4], Eq. (1.17))

$$E_{\rm h} = -\left(\mathbf{m}\cdot\mathbf{H}\right). \tag{13}$$

In the present case, where the magnetisation is modelled to be proportional to the magnetic field, the energy results in an additional bulk pressure term (where $m = \mu_0 M$ in a unit volume and $M = \chi H$ with χ the magnetic susceptibility)

$$E_{\rm h} = -\mu_0 M H = -\frac{1}{\chi\mu_0} m^2. \tag{14}$$

The general form of the dipolar interaction energy between dipoles with magnetic moments $\mathbf{m}_1$ and $\mathbf{m}_2$, respectively, and separated by $\mathbf{r}$, is given by ([4], Eq. (1.20))

$$E_{\rm dd} = \frac{1}{4\pi\mu_0}\left[\frac{\mathbf{m}_1\cdot\mathbf{m}_2}{r^3} - \frac{3}{r^5}\left(\mathbf{m}_1\cdot\mathbf{r}\right)\left(\mathbf{m}_2\cdot\mathbf{r}\right)\right]. \tag{15}$$

Assuming complete separation between the nonmagnetic and the magnetic fluid phase (which is the case in reality in contrast to the lattice Boltzmann model), the magnetic fluid phase of the model corresponds to a situation where identical and co-aligned dipoles with magnetic moment m are uniformly distributed over a lattice with unit lattice spacing. The interaction energy between two nearest neighbour dipoles on such a lattice are summarised in Figures 2a, b, c. The case where two dipoles are in line, one expects an attractive force between them, which is substantiated by the large negative contribution from the second term in the RHS of equation (15). In the case of the dipoles arranged side-by-side, on the other hand, that second term vanishes, and the positive contribution from

the first term remains, resulting in a repulsive force. Evaluating (15) (and dropping the universal factor $1/(4\pi\mu_0)$) for these two cases results in $E_{\rm dd} = -2m^2$ and $E_{\rm dd} = m^2$, respectively. The contribution from a dipole at a diagonal point with a distance of $r = \sqrt{2}$, is relatively small, $E_{\rm dd} = -2^{-5/2}m^2 = -0.18m^2$.

Since the force due to the dipolar interaction energy is $F = -\nabla E_{\rm dd}$, an interfacial pressure term can be defined as the difference between the energy acting on a dipole at the surface and an adjacent dipole just below the surface. Assuming a flat interface, the energy difference is given by one row of dipoles along the length of the interface. Calculating the dipolar interaction of such a row on a dipole at the surface, the interfacial pressure terms become

$$p_{\rm i,\parallel} = \frac{0.146}{4\pi\mu_0} m^2 \approx 0 \tag{16}$$

$$p_{\rm i,\perp} = \frac{-2.170}{4\pi\mu_0} m^2 \approx -\frac{m^2}{2\pi\mu_0}\,. \tag{17}$$

Thus, at the interface the pressure balance consists of the standard ('thermodynamic') pressure, p^σ, of the nonmagnetic fluid, $\sigma = 1$, on one side and of the combination of the 'thermodynamic' pressure, the 'bulk magnetic pressure' from equation (14), and the dipolar 'interfacial pressure' from equations (16) or (17) of the magnetic fluid, $\sigma = 0$ on the other side. Using the ideal gas equation, the density differences, $\delta\rho = \rho^0 - \rho^1$, should then scale as

$$\delta\rho_\parallel \propto \frac{m^2}{\chi\mu_0} \tag{18}$$

$$\delta\rho_\perp \propto \left(1 + \frac{\chi}{2\pi}\right)\frac{m^2}{\chi\mu_0}\,. \tag{19}$$

Comparing the pressure terms, (14) and (17), with the usual magnetic pressure terms it is evident that the term $\mu_0 MH$ corresponds to the bulk fluid magnetic pressure, $p_{\rm m} = \mu_0 \int M{\rm d}H$ ([4], Eq. (4.36b)), and the term $m^2/(2\pi\mu_0)$ to the magnetic normal pressure, $\frac{1}{2}\mu_0 M_n^2$, ([4], Eq. (5.23)). The magnetostrictive pressure,

$$p_{\rm s} = -\mu_0 \int_0^H \rho \left(\frac{\partial M}{\partial \rho}\right)_{H,T} {\rm d}H$$

([4], Eq. (4.36a)) cannot be represented by the present parameterisation of the magnetisation.

In the lattice Boltzmann model, where the external field is parameterised by the magnitude of the dipole moment, m, and where only the eight nearest neighbours contribute to the dipole interactions, the magnetic energy terms are completely described by the situations illustrated in Figures 2d, e, f, weighted by the factors ω_a defined in equation 4, leading to surface pressures, $p_{\rm m} = \Delta E_{\rm dd}$, of

$$p_{m,\perp} = -0.1013m^2$$

$$p_{m,\parallel} = +0.2320m^2.$$

Since the relationship between pressure and density in this model is $\rho = 3p$, the pressure balance becomes

$$\rho^0 + 3p_{\rm m} = \rho^1$$

which results, after inserting the magnetic surface pressure for the two cases, in expressions for the density difference across the two phases, $\delta\rho = \rho^0 - \rho^1$, as

$$\delta\rho_\perp = +0.3039m^2 \tag{20}$$

$$\delta\rho_\parallel = -0.6961m^2. \tag{21}$$

The density difference was tested with the lattice Boltzmann model for a range of values for m and two values for the separation constant, $\mathcal{G} = 2.0$ and 2.5. The results for three cases, all with $\mathcal{G} = 2.0$ are shown in Figure 3, the first with no magnetisation, the second with magnetisation perpendicular to the interface, and the last with the magnetisation parallel to the interface. The figures show clearly that in the absence of dipolar interactions, the densities in both phases are equal in contrast to the cases where dipolar interactions are present. If the applied magnetic field is normal to the interface, the density in the magnetic fluid increases, while it decreases when the field is parallel to the interface. Furthermore, it is evident that the effect is stronger in the case of the parallel applied field.

The scaling of the density difference with the magnetisation of the fluid, *i.e.* for different values of m, is best described by a quadratic in m, as demonstrated in Figure 4. The figure also shows that, while the value of $\mathcal{G}$ affects the densities in the two fluid phases, it has no significant effect on the density difference. Therefore, proportionality factors between $\delta\rho$ and m^2 were found for the combined results from both values of $\mathcal{G}$. The linear regression resulted in the expressions

$$\delta\rho_\perp = +\left(0.329 \pm 0.003\right) m^2 \tag{22}$$

$$\delta\rho_\parallel = -\left(0.732 \pm 0.009\right) m^2. \tag{23}$$

While these results lie outside the statistically calculated error margin compared to the predictions of 0.304 and -0.696, respectively, they are nevertheless very close. The small discrepancy might arise from the assumption in the derivation of the scaling that the interface is a true interface with pure fluid phases on both sides of the interface while the lattice Boltzmann model shows a residual presence of the magnetic fluid in the mainly non-magnetic phase and *vice versa*, as evident in Figure 3.

4 Drop deformation

Magnetic fluid drops elongate parallel to applied magnetic fields because of the anisotropy induced by the orientation of the magnetic moments of colloidal particles. For small amplitudes of the external magnetic field, these drops remain quite ellipsoidal, while becoming needle-like if the field is increased further [4,5]. In the case of 2D drops, their shape may be characterized through the eccentricity

$$\epsilon = \frac{a}{b} - 1 \tag{24}$$

where a and b are the major and minor axes of the ellipsis, respectively.

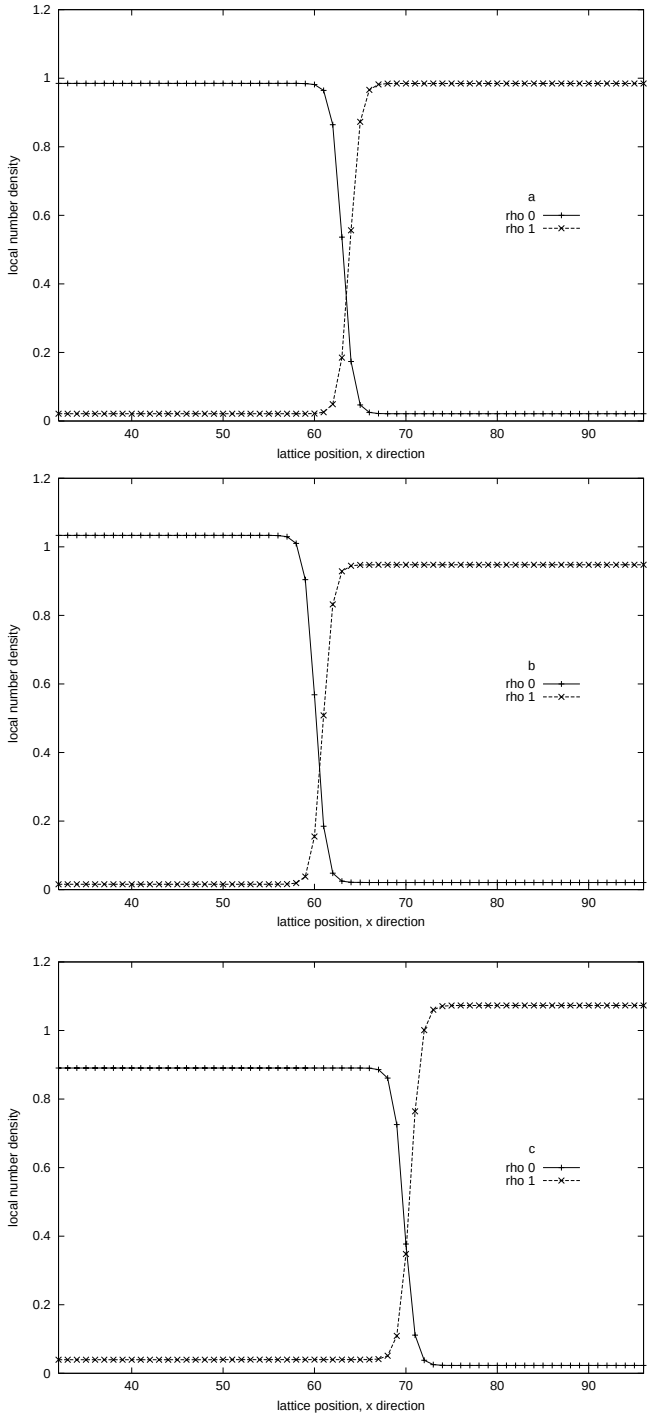

Fig. 3. Particle number density profiles across a linear interface at equilibrium: a) $m_x = 0$, $m_y = 0$; b) $m_x = 0.500$, $m_y = 0$; c) $m_x = 0$, $m_y = 0.500$.

A recent theoretical and experimental study on the elongation of magnetic fluid drops [18] revealed that, for small magnetic field amplitudes, the eccentricity of a 2D drop placed in a Hele-Shaw cell has a quadratic dependence on the field amplitude H (*i.e.*, on the fluid magnetisation M, since $M = \chi H$, where χ is the magnetic

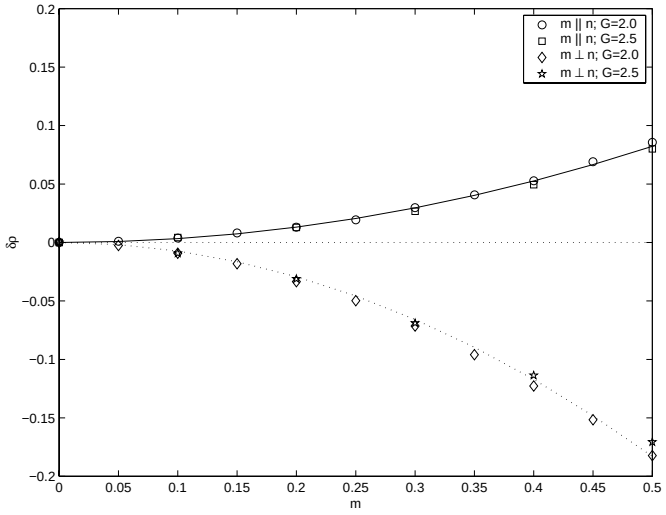

Fig. 4. Density difference between the magnetic and non-magnetic for different values of m_x ($\delta\rho_\perp$; solid line) or m_y ($\delta\rho_\parallel$; dotted line), respectively.

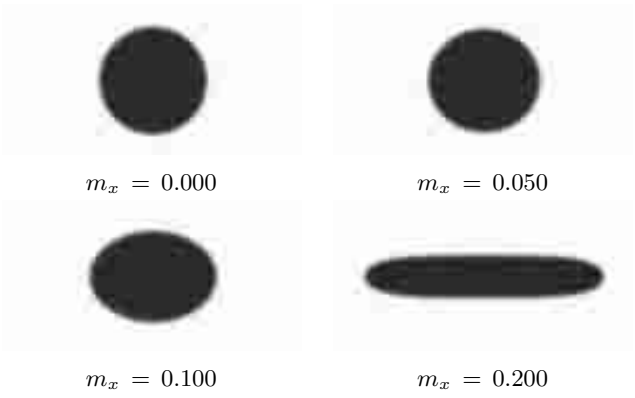

Fig. 5. Equilibrium shapes of magnetic fluid drops (lattice size 128×64) recovered after 20,000 automaton steps for $\mathcal{G} = 2.0$ and different values of the magnetic moment orientated along the x-axis.

fluid susceptibility)

$$\epsilon \propto \frac{\chi^2 H^2}{\gamma} \cdot \tag{25}$$

Here γ is the surface tension coefficient. To compare LB simulation results with those in [18], we consider that the magnitude of the magnetic moment **m** carried by our particles in the LB model may be seen as being proportional to the external magnetic field amplitude.

Figure 5 shows the equilibrium shape of a 2D magnetic fluid drop calculated with our LB model for different values of the magnetic moment **m** orientated along the x-axis. For small values of m_x, the magnetic fluid drop remains quite ellipsoidal, while it becomes needle-like at subsequently larger values.

For a quantitative investigation of the dependence of the drop eccentricity *vs.* magnetic field, we used a larger

lattice than in Figure 5. To compute the eccentricity in accordance to (24), we have to count the number of lattice nodes along the x- and y-axes, respectively, which are occupied by the magnetic fluid phase (a lattice node was considered to be occupied by the magnetic fluid phase when the value of ρ^0 was larger than 0.5). Although this procedure gives only an approximation of the interface position while the drop eccentricity is determined as the ratio of two integer numbers (a better approximation would be to use real numbers and an interpolation procedure instead of working with integer numbers to measure the length of the two axes of the ellipsis), a 144×96 lattice was found to provide accurate space resolution for our purposes, with a reasonable computing effort.

Figure 6 shows the LB computed dependence of the eccentricity, ϵ, of 2D magnetic fluid drops *vs.* the squared magnetic momentum, m^2, of particles belonging to species $\sigma = 0$, for two values of the interaction parameter $\mathcal{G}$. In all cases, simulations were started with the same circular drop of radius equal to 36 lattice units, while the x component of the magnetic moment $\mathbf{m}$ was set to different values. The quite linear dependence of ϵ on m^2, which is seen for small values of m is remarkable, despite the very simple LB model we used.

As m increases, on can see the LB computed eccentricity values in Figure 6 becomes larger than the value one would expect in accordance to the $\epsilon \propto m^2$ prediction. This behaviour may be explained since the drops become more flattened when approaching the needle-like status where the thickness of the drops becomes uniform except at the extremities.

The fact that data points we get using $\mathcal{G} = 1.5$ in Figure 6 are situated above the points corresponding to $\mathcal{G} = 2.0$ is also in accordance to the theoretical estimation (25) derived in [18] since the surface tension coefficient decreases when $\mathcal{G}$ also decreases [7,10]. The fact that a larger amount of magnetic particles is dispersed in the non-magnetic phase (*i.e.*, outside the drop) for smaller $\mathcal{G}$ may account for the deviations of the resulting eccentricity values from the corresponding straight lines passing through the origin, which are more evident for $\mathcal{G} = 1.5$.

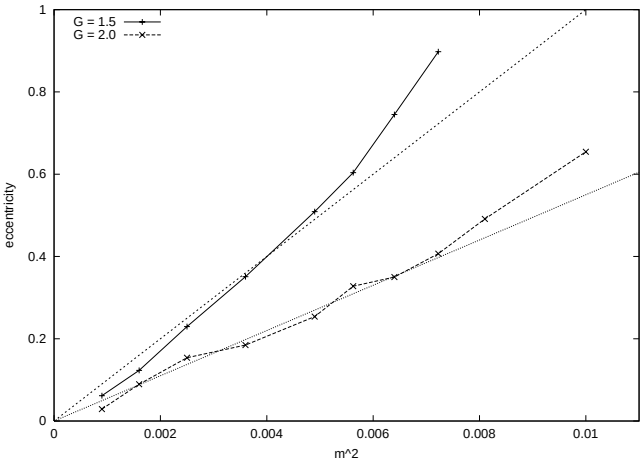

Fig. 6. Eccentricity of magnetic fluid drops as a function of the squared magnetic moment of particles (m^2) belonging to species $\sigma = 0$, for $\mathcal{G} = 1.5$ and $\mathcal{G} = 2.0$ (upper and lower data sets, respectively). The straight lines are eye guides.

5 Normal field instability

A perpendicular, uniform magnetic field applied to a pool of magnetic fluid generates an ordered pattern of surface protuberances when the field exceeds a critical value. The stability analysis of the magnetic fluid surface gives the following dispersion relation for a perturbation wave in the absence of the gravitational field [4]:

$$\omega^2(\rho^0 + \rho^1) = \gamma\kappa^3 - \frac{\kappa^2\mu_0 M^2}{1 + \mu_0/\mu} \qquad (26)$$

where ω is the complex angular frequency, κ is the wave number, γ is the surface tension coefficient, M is the magnetic fluid magnetisation, while μ_0 and μ are the magnetic permeabilities of the vacuum and the magnetic fluid, respectively.

In order to see the ability of the present LB model to capture the main characteristics of the development of normal field instabilities, in Figures 7 and 8 we show the results of computer runs made on two lattices having 64×128 and 128×128 nodes, respectively, but otherwise identical conditions, namely the interaction constant $\mathcal{G} = 2.0$, no tangential magnetisation ($m_x = 0$), and a normal magnetisation of $m_y = 0.35$. Periodic boundary condition were used in the x-direction, while bounce back walls were introduced at the upper and lower lattice boundaries. A perturbation, $A\sin(2\pi i/L)$ with $i = 0, 1, \ldots, L-1$ where $L = 64$ or $L = 128$, respectively, was superimposed on the flat magnetic fluid interface located at the middle of the lattice. While the parameters corresponding to the surface tension, the magnetic permeabilities, and the magnetisation in equation (26) remain the same, the change in the lattice geometry and imposed perturbation corresponds to a change in the wave number, κ.

Both simulations show the formation of oscillating magnetic fluid spikes orientated along the external magnetic field (*i.e.*, normal to the interface). In the first case (Fig. 7), however, the amplitude of these spikes is attenuated until the interface recovers the equilibrium plane shape (not shown in Fig. 7) after a large number of time steps (approx. 50,000). In the second case (Fig. 8), oscillations increase their amplitude very quickly due to the normal field instability. The large values of the resulting fluid velocities open up the possibility of further, shear-induced instabilities of Kelvin-Helmholtz type, which may be the cause for the wave-like structure of the peaks at later stages. The extremely intricate structure resulting from the instability is not shown in Figure 8 since this later stage does not correspond to the physical situation in which the spikes equilibrate with a stable shape [4]. Our attempts to increase the surface tension (which eventually would eliminate the development of the later stage instability) using larger values of the interaction constant $\mathcal{G}$ during computer runs failed because the fluid system

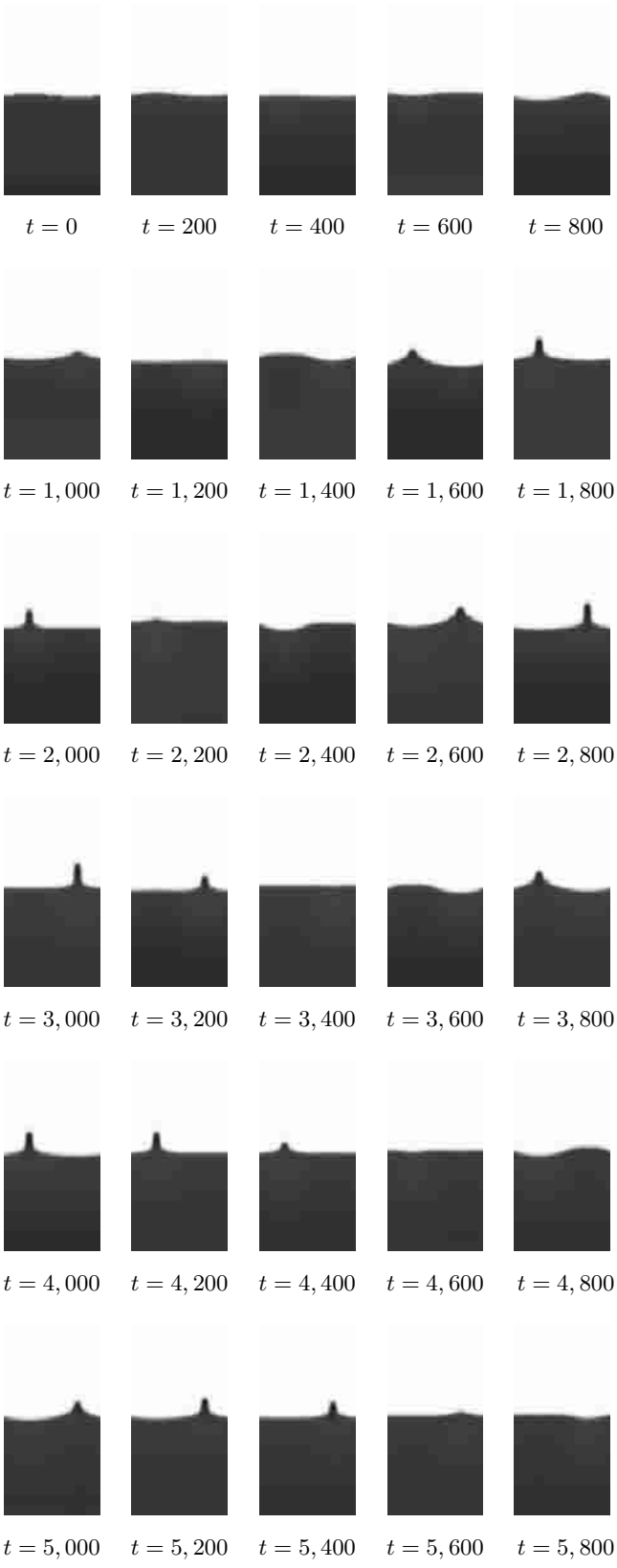

Fig. 7. Time evolution of a perturbed magnetic fluid interface under normal field ($\mathcal{G} = 2.0$, $m_x = 0$, $m_y = 0.35$, initial amplitude of the perturbation: 2 lattice units, lattice size: 64×128).

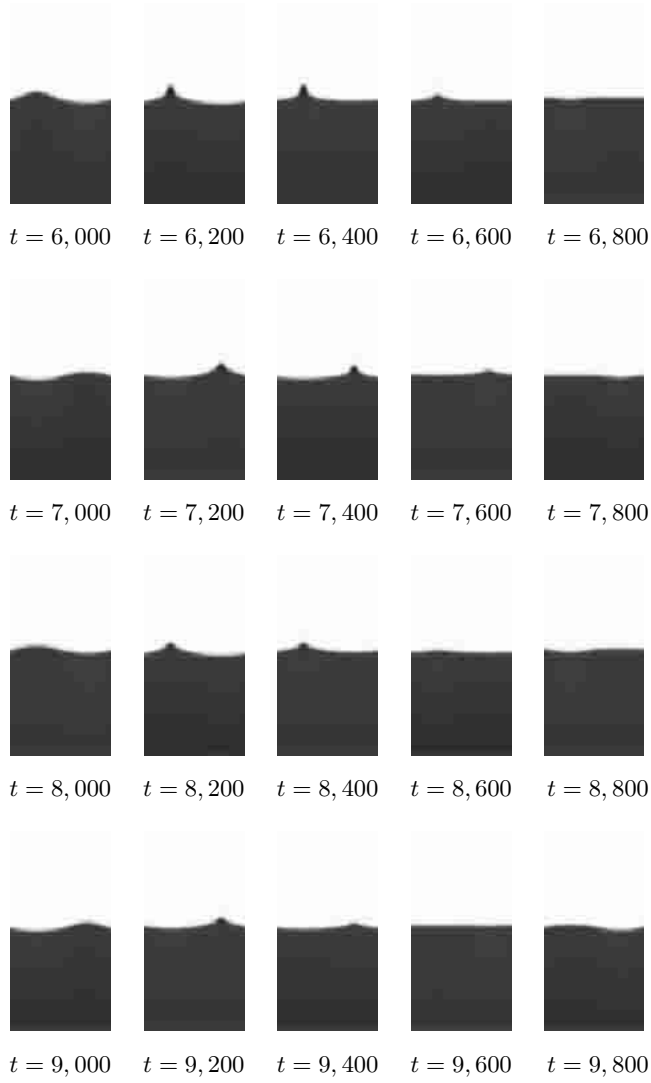

Fig. 7. Continued.

becomes unstable when $\mathcal{G} > 3$ and negative values of the distribution functions are recovered.

While at present no exact mapping between the representation of the model interactions (phase separation and dipolar interactions) and the quantities of equation (26) (surface tension and magnetisation) can be formulated, a qualitative explanation for the different behaviour can be found in the dispersion relation for the normal instability, equation (26) [4]. In the first case ($L = 64$) the wavevector $\kappa = 2\pi/L$ is large enough to ensure a real value of the angular frequency ω in equation (26), which means that the perturbation is finally attenuated. This is no more valid in the second case, when the occurrence of an imaginary value of the frequency ω allows the perturbation to develop further. For a direct comparison between the model and the dispersion relation, a much larger number of simulations are required which will for the subject of a separate paper.

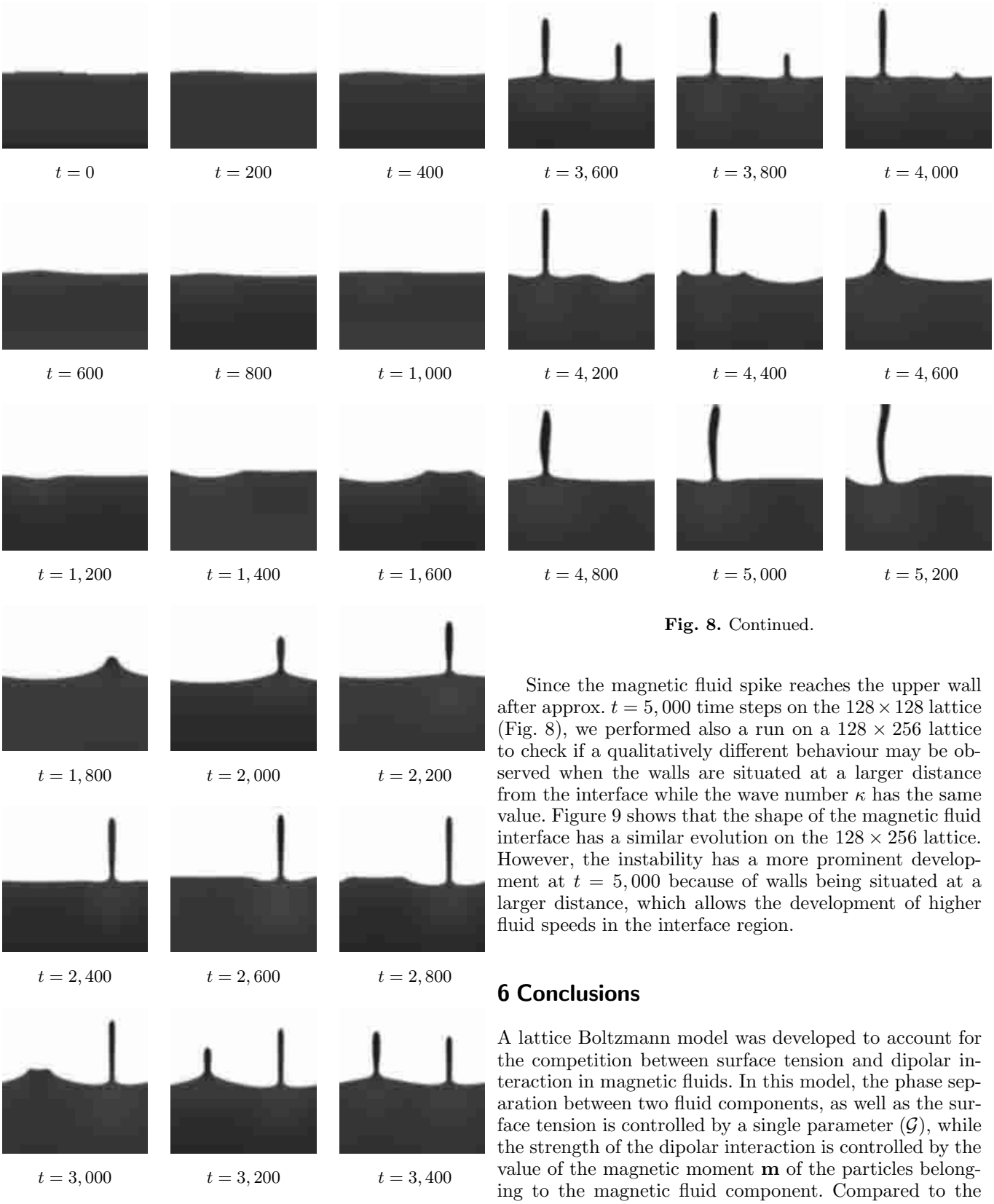

Fig. 8. Time evolution of a perturbed magnetic fluid interface under normal field ($\mathcal{G} = 2.0$, $m_x = 0$, $m_y = 0.35$, initial amplitude of the perturbation: 2 lattice units, lattice size: 128×128).

Fig. 8. Continued.

Since the magnetic fluid spike reaches the upper wall after approx. $t = 5,000$ time steps on the 128×128 lattice (Fig. 8), we performed also a run on a 128×256 lattice to check if a qualitatively different behaviour may be observed when the walls are situated at a larger distance from the interface while the wave number κ has the same value. Figure 9 shows that the shape of the magnetic fluid interface has a similar evolution on the 128×256 lattice. However, the instability has a more prominent development at $t = 5,000$ because of walls being situated at a larger distance, which allows the development of higher fluid speeds in the interface region.

6 Conclusions

A lattice Boltzmann model was developed to account for the competition between surface tension and dipolar interaction in magnetic fluids. In this model, the phase separation between two fluid components, as well as the surface tension is controlled by a single parameter ($\mathcal{G}$), while the strength of the dipolar interaction is controlled by the value of the magnetic moment $\mathbf{m}$ of the particles belonging to the magnetic fluid component. Compared to the forces present in a complete ferrohydrodynamic description, this model is such a simplification that there is no *a priori* certainty that it should be sufficient to describe the range of different situations presented here. Despite its

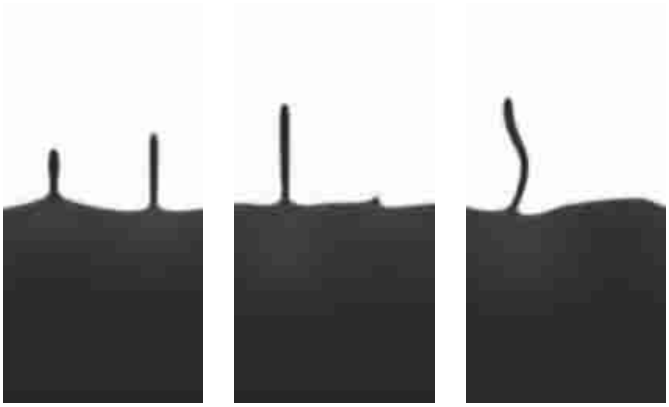

$t = 3,200$ $t = 4,000$ $t = 5,000$

Fig. 9. Shape of the magnetic fluid interface under normal field ($\mathcal{G} = 2.0$, $m_x = 0$, $m_y = 0.35$, initial amplitude of the perturbation: 2 lattice units) after 3, 200, 4, 000 and 5,000 time steps performed on the 128×256 lattice.

simplicity, the model is able to recover the main characteristics of a 2D magnetic liquid - nonmagnetic fluid interface: drop deformation under the action of an external magnetic field and the early stage development of normal field instability. The success of the model in the systems studied supports our view that this very simple model, representing only phase separation and dipolar interactions, contains the essential dynamics for magnetic-nonmagnetic two-fluid systems. As shown below, discrepancies between the model and a ferrohydrodynamic description could easily be identified giving clear indications to the additional forces required to reproduce a given situation. Therefore, shortcomings provide useful physical insight into the relative importance of the range of forces contained in the full equations of motion.

Since the two fluid components are not perfectly immiscible (a characteristics which is present also in more elaborated LB models [15–17]), the region of the domain representing the nonmagnetic phase contains some magnetic fluid particles and *vice versa*. Despite this unphysical representation, interface forces and phenomena are well captured by the model. The use of an ideal gas representation of two immiscible liquids seems therefore justified in the presented situations.

The most obvious differences between the behaviour based on a continuum description and that based on the lattice Boltzmann model arose through the parameterisation of the magnetisation of the magnetic particles by an externally imposed magnetic field and through the description of the dipolar interaction. The very much simplified description of the magnetisation of the magnetic fluid resulted in the absence of the magnetic bulk pressure. It would, however, be easily possible to expand the present model to incorporate a representation of the magnetic fluid pressure, based on equation (14). The restriction of the dipolar interaction to the nearest neighbours–a logical consequence of using a lattice Boltzmann approach–resulted in a quantitative difference compared to the case where dipoles at a larger distance were included. A possible extension of the model might be to balance the 'absent' distant dipoles in a local manner by assigning 'mirror' dipolar charges to the non-polar fluid. By acting only on the dipolar fluid phase, no unphysical effects on the non-polar phase would be added, and because the forces are localised to the nearest neighbours, such an extension would only be noticed by the dipolar phase at the interface. This idea, however, requires further work.

This work was supported by the European Community TRACS (Training and Research on Advanced Computing Systems) Programme, which is part of the Access to Research Infrastructure Action of the Improving Human Potential Programme. Computer runs were done at the Edinburgh Parallel Computing Centre (EPCC). V.S. would like to acknowledge Dr. W.-G. Früh for hosting him at Heriot-Watt University, as well as Dr. J.C. Desplat, Catherine Inglis and many other people at EPCC (The University of Edinburgh), for their helpful assistance.

References

1. D.H. Rothman, S. Zaleski, *Lattice - Gas Cellular Automata, Simple Models of Complex Hydrodynamics* (Cambridge University Press, Cambridge, 1997).
2. B. Chopard, M. Droz, *Cellular Automata Modeling of Physical Systems* (Cambridge University Press, Cambridge, 1998).
3. D.A. Wolf-Gladrow, *Lattice Gas Cellular Automata and Lattice Boltzmann Models: An Introduction* (Springer Verlag, Berlin, 2000).
4. R.E. Rosensweig, *Ferrohydrodynamics* (Cambridge University Press, Cambridge, 1985).
5. *Magnetic Fluids and Applications Handbook*, UNESCO Series of Learning Materials, edited by B. Berkovsky, V. Bashtovoi (Begell House Inc., New York, 1996).
6. *Proceedings of the 8th International Conference on Magnetic Fluids, June 29 – July 3, 1998, Timişoara, Romania*, edited by I. Anton, L. Vékás, V. Sofonea (North Holland, Elsevier, Amsterdam, 1999): special issue of J. Magn. Magn. Mater. **201** (1999).
7. X. Shan, H. Chen, Phys. Rev. E **47**, 1815 (1993).
8. Y.H. Qian, D. D'Humières, P. Lallemand, Europhys. Lett. **17**, 479 (1992).
9. X. He, L.S. Luo, Phys. Rev. E **56**, 6811 (1997).
10. N. Martys, H. Chen, Phys. Rev. E **53**, 743 (1996).
11. B.R. Sehgal, R.R. Nourgaliev, T.N. Dinh, Prog. Nucl. Energy **34**, 471 (1999).
12. H. Xi, C. Duncan, Phys. Rev. E **59**, 3022 (1999).
13. V. Sofonea, Europhys. Lett. **25**, 390 (1994).
14. L.E. Reichl, *A Modern Course in Statistical Physics* (Edward Arnold Pubishers Ltd., London, 1980).
15. E. Orlandini, M.R. Swift, J.M. Yeomans, Europhys. Lett. **32**, 463 (1995).
16. M.R. Swift, E. Orlandini, W.R. Osborn, J.M. Yeomans, Phys. Rev. E **54**, 5041 (1996).
17. K. Langaas, J. Yeomans, Eur. Phys. J. B **15**, 133 (2000).
18. S. Banerjee, M. Fasnacht, S. Garoff, M. Widom, Phys. Rev. E **60**, 4272 (1999).